AIAA JOURNAL
Vol. 39, No. 12, December 2001

Far-Field Calculations for Turbofan Noise

Indranil Danda Roy* and Walter Eversman†
University of Missouri–Rolla, Rolla, Missouri 65409

The development of variable-order mapped infinite wave envelope elements for finite element modeling of acoustic radiation from turbofan nacelles is reviewed. These elements can be used outside of the near field as a nonreflecting boundary condition and as a finite-dimensional discretization of the infinite exterior domain for calculation of far-field acoustic radiation. The Kirchhoff method previously has been investigated in the context of the turbofan inlet radiation problem to extend a near-field solution to the far field. When the results of the mapped infinite wave envelope element analysis are compared with results of the Kirchhoff method, it is found that the mapped element formulation efficiently provides the acoustic far field, obviating the need to carry out an additional Kirchhoff integral formulation. Relative efficiencies are considered, and it is found that finite-dimensional discretization of the far field using mapped infinite elements is superior to the Kirchhoff formulation when radiation directivity in the entire far field is required.

Introduction

MODELING of acoustic radiation is complicated by the requirements that prediction of the acoustic field is required in some finite subdomain of an infinite domain. This requires that computations be limited to the subdomain with a nonreflecting boundary or that the infinite domain be mapped onto a finite computational domain. In case of finite element modeling, this has led to wave envelope elements[1,2] and mapped infinite wave envelope elements.[3–6] Mapped infinite wave envelope elements map the infinite domain to a finite domain. Standard wave envelope elements restrict computations to a large but finite domain bounded by a Sommerfeld radiation condition on an outer boundary that is reached from an inner standard finite element domain via large elements in which the shape functions are augmented to reflect decay with distance from the source and the temporal and spatial character of outgoing waves. For the turbofan engine inlet, Parrett and Eversman[1] and Danda Roy and Eversman[2] have developed computational models to determine the noise radiated to the far field. In their studies, a wave envelope analysis has been incorporated into the standard finite element model (FEM) for far-field approximation. Mapped infinite wave envelope elements have been investigated extensively for acoustic radiation in a stationary medium. These elements have some distinct advantages over standard wave envelope elements. In the case of harmonic radiation, the most significant is the possibility of adjusting the order of the elements to fit the requirements of the problem. Careful examination of the shape function of mapped infinite wave envelope elements reveals that they can be introduced well into what would normally be considered the acoustic near field, reducing mesh refinements and dimensionality. In contrast, standard wave envelope elements can be introduced only at a distance far enough from the acoustic source where it can be approximated by a monopole in uniform flow. A second advantage of the mapped infinite wave envelope formulation is that the Sommerfeld radiation boundary is infinitely far away and is never explicitly appended as a natural boundary condition.

The study reported here reviews the use of variable-order mapped infinite wave envelope elements in connection with aeroacoustic problems related to turbofan acoustic radiation, previously reported by Eversman.[5,6] A combined FEM and Kirchhoff integral method has been investigated in the context of the turbofan inlet radiation problem as a means of projecting the near-field acoustic solution to the far field. Farassat and Myers[7] have formulated the Kirchhoff method for moving and deformable surfaces, and it has been utilized by Ozyoruk and Long[8] in computing the acoustic far field from information generated in the near field using a finite difference discretization of the field equations. Spence[9] developed a hybrid technique that couples the FEM/wave envelope element analysis used in turbofan inlet acoustic radiation calculations by Parrett and Eversman[1] and Danda Roy and Eversman[2] with a Kirchhoff integral formula. Here the approach of Spence[9] is modified to use a radiation code that implements mapped infinite elements to provide a reflection free boundary and model the far field. The radiation code is executed first to define the acoustic pressure and its spatial and temporal derivatives on a user-defined Kirchhoff surface. In this case the surface happens to be the transition boundary between standard finite elements and mapped infinite wave envelope elements. Once the acoustic parameters on the Kirchhoff surface are defined, the Kirchhoff formula is integrated over the entire Kirchhoff surface to obtain the acoustic pressure at observer locations in the far field. The method is based on evaluation of an integral depending only on the information on the Kirchhoff surface and the location of the observer. It does not require the calculation of the entire acoustic field to evaluate the acoustic pressure at a few observer locations.

This investigation has two main goals. The first is to demonstrate that an FEM formulation for turbofan acoustic radiation using mapped infinite wave envelope elements to close the computational domain also provides an efficient method for the determination of far-field acoustic pressure radiation beyond the computational domain. The second goal is to integrate the Kirchhoff integral formulation within the framework of a turbofan acoustic radiation code that uses mapped elements. This is an extension of the work of Spence,[9] making use of an improved radiation code. With the Kirchhoff implementation, it is possible to compare far-field calculations based on simple postprocessing of FEM/mapped element calculations with those obtained by postprocessing based on the Kirchhoff formulation. A measure of relative accuracy of the two methods will be addressed by direct comparison of results. Relative efficiency of the two approaches also will be considered. The Kirchhoff integral formulation requires additional postprocessing, first to obtain acoustic pressure and required derivatives on the Kirchhoff surface and then to carry out the prescribed integration. Numerical experiments will compare computational cost using the Kirchhoff method and using the FEM/mapped element approach in cases when only a few observer points are used and when an extensive far-field radiation field is to be produced.

Received 4 June 1999; revision received 25 June 2001; accepted for publication 26 June 2001.

*Graduate Student, Department of Mechanical and Aerospace Engineering and Engineering Mechanics; currently Research Engineer, Powertrain Noise, Ford Motor Company, Dearborn, MI 48121.

†Curators' Professor, Department of Mechanical and Aerospace Engineering and Engineering Mechanics. Associate Fellow AIAA.

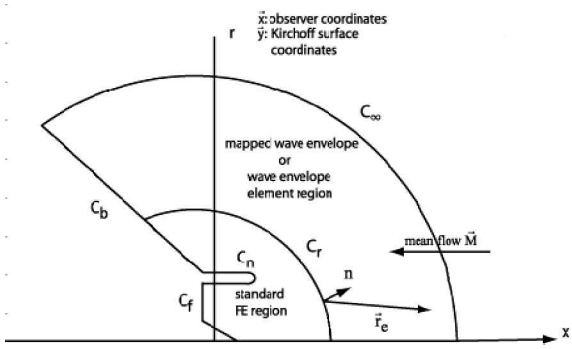

Fig. 1 FEM computational region showing near and far fields.

FEM Modeling of Turbofan Inlet Acoustic Radiation

An extensive description of the formulation and computational scheme for acoustic radiation from a turbofan engine inlet has been provided by Parrett and Eversman[1] and Danda Roy and Eversman.[2] Details relevant to the current developments are discussed here. In this model, the nacelle geometry and the steady flowfield (representing flow into the inlet and forward flight) are assumed to be axially symmetric. The noise source is assumed to be harmonic in time and is decomposed into its angular modal content, allowing a two-dimensional representation of the acoustic field in a plane through the nacelle axis of symmetry. The solution domain is shown in Fig. 1. It is the x, r plane in cylindrical coordinates. The source plane is designated by C_f. The source is input on this plane by specifying complex amplitudes of incident duct modes.[2] The nacelle surface is C_n. On this boundary, steady flow velocity has a vanishing normal component as does acoustic particle velocity on acoustically hard surfaces. An impedance boundary condition also can be represented on appropriate portions of C_n. An artificial baffle C_b formed by a ray from the origin limits the solution domain. The sweep angle for the baffle is chosen in such a way that minimal effect on the acoustic field is created.[10] The domain of computation is divided into two parts. In an inner region where the steady mean flow is nonuniform, a standard finite element mesh is used, composed of eight-node serendipity elements with a resolution of four to five elements per wavelength. The near field is terminated on a transition boundary C_r beyond which far-field elements are used. The boundary C_r should be placed far enough from the inlet so that the steady mean flow outside it is essentially uniform (representing the forward flight effect). In earlier studies[1,2] this outer region was large but finite and bounded by C_∞, a circle representing a constant phase surface for an acoustic source located at the origin. On this boundary, a Sommerfeld radiation condition was specified. Wave envelope elements[1,2] were used in this region to reach the outer boundary C_∞ with minimal cost in mesh refinement.

In a second implementation of acoustic radiation codes,[5,6] the far-field region is extended to infinity, and a single layer of mapped infinite wave envelope elements is used to provide a reflection-free boundary on C_r and to compute the acoustic field in the far field as required. The boundary C_∞ is not part of the solution.

The starting point for the formulation of both the steady mean flow and the acoustic perturbation consists of the inviscid mass and momentum equations and the energy equation in the form of isentropic equation of state. The acoustic field equations are obtained by considering small perturbations on a steady irrotational mean flow. This formulation makes it possible to introduce mean flow and acoustic perturbation velocity potentials. Acoustic perturbations in pressure, density, and velocity potential are harmonic in time and in the angular coordinate of the form $p(x,r)e^{i(\eta_r t - m\theta)}$, $\rho(x,r)e^{i(\eta_r t - m\theta)}$, and $\phi(x,r)e^{i(\eta_r t - m\theta)}$, where η_r is the nondimensional source frequency, m is the angular mode number, and θ is the circumferential angle about the inlet axis in a cylindrical axis system. In linearized form, the weak formulation is[1,2]

$$\iiint_V \{\nabla W \cdot (\rho \nabla \phi + \rho \nabla \phi_r) - i\eta_r W \rho\}\, \mathrm{d}V = \iint_S W(\rho_r \nabla \phi + \rho \nabla \phi_r) \cdot \boldsymbol{n}\, \mathrm{d}S \tag{1}$$

Weighting functions are taken as $W(x,r,\theta) = W(x,r)e^{im\theta}$. Angular harmonics proportional to $e^{-im\theta}$ represent the decomposition of the solution periodic in θ in a Fourier series. The angular mode number m is a parameter of the solution. The surface integral is over all surfaces bounding the domain. The unit normal $\boldsymbol{n}$ for the surface integral is out of the domain at the surface in question. The weak formulation continues with the linearized momentum equation

$$\rho = -\left(\rho_r / c_r^2\right)(i\eta_r \phi + \nabla \phi_r \cdot \nabla \phi) \tag{2}$$

which is used to replace ρ in Eq. (1). The linearized equation of state

$$p = c_r^2 \rho \tag{3}$$

is used to produce an alternative form of the momentum equation in terms of acoustic pressure:

$$p = -\rho_r (i\eta_r \phi + \nabla \phi_r \cdot \nabla \phi) \tag{4}$$

The acoustic particle velocity and acoustic velocity potential are related according to

$$\boldsymbol{v} = \nabla \phi \tag{5}$$

The linearization process also produces the weighted residual formulation for the steady flow

$$\iiint_V \nabla W \cdot (\rho_r \nabla \phi_r)\, \mathrm{d}V = \iint_S W(\rho_r \nabla \phi_r) \cdot \boldsymbol{n}\, \mathrm{d}S \tag{6}$$

and the steady flow momentum equation in terms of the speed of sound,

$$c_r^2 = 1 - [(\gamma - 1)/2]\left[\nabla \phi_r \cdot \nabla \phi - M_\infty^2\right] \tag{7}$$

and in terms of the steady flow density,

$$\rho_r = \left\{1 - [(\gamma - 1)/2]\left(\nabla \phi_r \cdot \nabla \phi - M_\infty^2\right)\right\}^{1/(\gamma - 1)} \tag{8}$$

Equations (1–8) are in nondimensional form, where ϕ is the acoustic potential, ϕ_r is the local mean flow (reference) potential, ρ is the acoustic density, ρ_r is the local mean flow density, p is the acoustic pressure, and c_r is the local speed of sound in the mean flow. All quantities are made nondimensional by using the density in the far field ρ_∞, the speed of sound in the far field c_∞, and a reference length that is defined as the duct radius at the source plane, R, where acoustic modes are defined. All quantities are nondimensional. $M_\infty = M_0$ is the Mach number in the far field representing the forward flight effect.

The surface integral in Eq. (1) provides the boundary condition on the duct walls and at the source. The acoustic source is specified by the complex amplitudes of acoustic duct modes at the source plane. On this plane, FEM nodal values of acoustic potential are replaced by complex amplitudes of the acoustic potential modes by an eigenfunction expansion. Incident acoustic modal amplitudes are input and reflected modal amplitudes are computed as part of the solution. Details of this procedure are available in the previous work.[1,2]

A previous study of the turbofan inlet radiation problem[10] showed that the baffle can be positioned to produce practically no effect on typical acoustic radiation patterns. Therefore, there is little contribution from the surface integral on the baffle. Furthermore, in the case of mapped infinite wave elements, the surface integral is never explicitly introduced on a far-field boundary because the assumed form of solution in the outer region implicitly satisfies the Sommerfeld condition. In the steady flow near field (inside the transition boundary C_r), where the flow is nonuniform, the weak formulation is discretized using standard finite element techniques. Example calculations presented in this study are based on two-dimensional rectangular isoparametric serendipity elements with eight nodes. In the steady flow far field, where the flow is essentially uniform, mapped infinite wave envelope elements are introduced to obtain closure of the computational domain.

Mapped Infinite Wave Envelope Element Formulation

Infinite Mapping

Important features of the introduction of the mapped infinite wave envelope element to discretize the far acoustic field are most easily visualized by comparing to a standard finite element discretization. A common FEM discretization in two dimensions uses a mesh composed of elements that are curvilinear quadrilaterals. These quadrilateral elements are mapped from a parent quadrilateral on $-1 \le \xi \le 1$ and $-1 \le \eta \le 1$ as shown in Fig. 2 for an element with eight nodes. Mappings are of the form

$$x = [N(\xi, \eta)]\boldsymbol{x}, \qquad r = [N(\xi, \eta)]\boldsymbol{r} \tag{9}$$

where $[N(\xi, \eta)]$ is an interpolation (row) matrix, with components $N(\xi, \eta)$ and $\boldsymbol{x}$ and $\boldsymbol{r}$ are vectors of nodal values of x and r. Equation (9) maps points ξ and η in the parent element to points x and r in the global curvilinear quadrilateral element. Mapping functions are typically polynomials. The eight-node case shown would correspond to quadratic polynomials in ξ and η. This mapping is used in the standard finite element region. Finite element operations implied in Eq. (1) are formulated in the physical x and r domain, but carried out via the mapping in the parent element ξ and η domain.

In the far field, the global element is restricted in its geometry as shown in Fig. 3. The geometry is suited for representing propagation that is essentially outward from the source. The element is bounded by the surface C_r on which it conforms with the conventional finite element of the inner region. The edges of the element are straight lines (rays), extending outward more or less radially, though not necessarily from the axis system origin nor necessarily from a common origin. To conform with eight-node (quadratic) elements described earlier, a third radial line between the two edges is required. A ray of an element has an apparent origin at a point x_0 and r_0 which in general can be different for each ray. The element again maps to a parent element in the ξ and η plane, $-1 \le \xi \le 1$ and $-1 \le \eta \le 1$ as shown in Fig. 3. The rays of the element map to the ξ axis with $\eta = -1, 0, 1$ in the parent element according to

$$x - x_0 = [-2\xi/(1-\xi)](x_1 - x_0) + [(1+\xi)/(1-\xi)](x_2 - x_0) \tag{10}$$

$$r - r_0 = [-2\xi/(1-\xi)](r_1 - r_0) + [(1+\xi)/(1-\xi)](r_2 - r_0) \tag{11}$$

The node x_1, r_1 is coincident with a node in the conventional element with which it conforms on the boundary C_r. The mapping is simplified if the node at x_2, r_2 is located such that $x_2 - x_0 = 2(x_1 - x_0)$ and $r_2 - r_0 = 2(r_1 - r_0)$. In this case

$$x - x_0 = \frac{2(x_1 - x_0)}{1-\xi}, \qquad r - r_0 = \frac{2(r_1 - r_0)}{1-\xi} \tag{12}$$

The mapping has the properties that $\xi = -1$ maps to $x = x_1, r = r_1$ (the coordinates of the element nodes on C_r), $\xi = 0$ maps to $x_2 - x_0 = 2(x_1 - x_0)$ and $r_2 - r_0 = 2(r_1 - r_0)$, and $\xi = 1$ maps to $x = \infty$ and $r = \infty$. The mapping along a ray thereby transforms the infinite domain in the physical coordinates to the domain $-1 \le \xi \le 1$ in the parent element. The mapping is completed by a conventional mapping, for example, quadratic, on $-1 \le \eta \le 1$. The element shown in Fig. 3 has six mapping nodes. Returning to the representation of the mapping in the case of conventional elements of Eq. (9), a similar representation is used here:

$$x = [M(\xi, \eta)]\boldsymbol{x}, \qquad r = [M(\xi, \eta)]\boldsymbol{r} \tag{13}$$

where $[M(\xi, \eta)]$ is a row vector of element mapping functions $M_i(\xi, \eta)$ and $\boldsymbol{x}$ and $\boldsymbol{r}$ are vectors of nodal values of x and r at element nodes. Equation (13) maps points ξ and η in the finite parent element

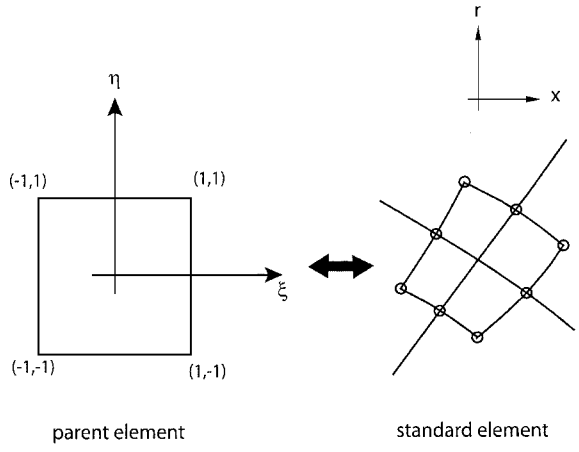

Fig. 2 Standard element mapping.

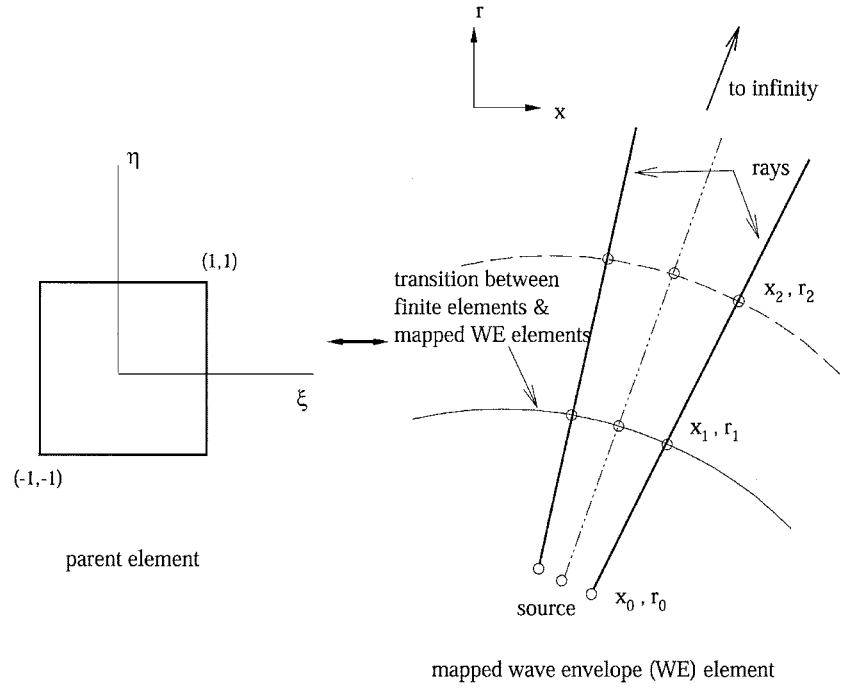

Fig. 3 Mapping summary for mapped infinite elements.

to points x and r in the global element, infinite in the outward direction. Mapping functions are combinations of the infinite mapping functions, Eqs. (10–12) and conventional polynomial mapping functions. Details are found in Refs. 3 and 4.

Shape Functions

In the region of standard finite elements, element interpolation functions (shape functions) are the same as element mapping functions, that is, for example, in terms of acoustic potential,

$$\phi = [N(\xi, \eta)]\phi \tag{14}$$

where ϕ is a vector of nodal values of acoustic potential $\phi(x, r)$. Weighting functions $W(x, r)$, discussed following Eq. (1), are interpolated in the same way. This type of element is referred to as isoparametric.

Shape functions in the mapped elements are constructed to display the characteristics of the acoustic field at large distances from the source in the form[5,6]

$$\phi = Q(\boldsymbol{x})e^{im\theta} R_1 \frac{\exp\{-i\eta_r[\psi(\boldsymbol{x}) - \psi_1]\}}{R(\boldsymbol{x})} = R(\boldsymbol{x})e^{-im\theta}e^{-i\mu(x)}$$

$$\phi = P(\boldsymbol{x})e^{-im\theta}e^{-i\mu(x)} \tag{15}$$

where $\boldsymbol{x} = (x, r)$ and

$$R = \sqrt{(x - x_0)^2 + \beta^2(r - r_0)^2} = 2R_1/(1 - \xi) \tag{16}$$

$$R_1 = \sqrt{(x - x_0)^2 + \beta^2(r - r_0)^2} \tag{17}$$

$$\beta^2 = 1 - M^2 \tag{18}$$

where M is the Mach number of the uniformly flowing medium. Here $\mu(\boldsymbol{x})$ is the phase relative to the transition surface C_r, defined by

$$\mu(\boldsymbol{x}) = \eta_r[\psi(\boldsymbol{x}) - \psi_1] \tag{19}$$

$$\psi = (1/\beta^2)[-M(x - x_0) + R] = 2\psi_1/(1 - \xi) \tag{20}$$

where

$$\psi_1 = (1/\beta^2)[-M(x_1 - x_0) + R_1] \tag{21}$$

The function $P(\boldsymbol{x})$ in Eq. (15), defined by

$$P(\boldsymbol{x}) = Q(\boldsymbol{x})[R_1/R(\boldsymbol{x})] \tag{22}$$

should at large distances from the apparent acoustic source display the appropriate asymptotic behavior with distance consistent with a multipole of specified order. In addition it should have capability of accounting for near-field effects and should conform to interpolation in conventional elements on the interface C_r. The phase function $\mu(\boldsymbol{x})$ should asymptotically represent outward acoustic radiation at large distances from the apparent source.

In terms of the ξ and η coordinates of the parent element, $\mu(\boldsymbol{x})$ and $R(\boldsymbol{x})/R_1$ have simple forms suggested by Eqs. (10) and (11):

$$\mu(\xi, \eta) = \psi_1[(1 + \xi)/(1 - \xi)] \tag{23}$$

$$R_1/R(\xi, \eta) = \tfrac{1}{2}(1 - \xi) \tag{24}$$

The function $p(\boldsymbol{x})$ in the mapped infinite wave envelope element can be represented by standard FEM interpolation:

$$P(\xi, \eta) = [R_1/R(\xi, \eta)][S(\xi, \eta)]\boldsymbol{Q} = [N(\xi, \eta)]\boldsymbol{Q} \tag{25}$$

where $\boldsymbol{Q}$ is a vector of nodal values of the function $Q(\boldsymbol{x})$ and $S_i(\xi, \eta)$ is the shape function corresponding to node i in the element. There are six nodes involved in the infinite mapping, and these can be used in the interpolation of $Q(\boldsymbol{x})$. It will generally be appropriate to use more than the mapping nodes by including extra nodes along the rays.[5,6]

In general, the composite shape function $N_i(\xi, \eta)$ can be constructed from the qth-order Lagrangian shape function for node i, $L_i^q(\xi, \eta)$ (q is the number of interpolation nodes along the ξ axis) according to

$$N_i(\xi, \eta) = \tfrac{1}{2}(1 - \xi)L_i^q(\xi, \eta) \tag{26}$$

Along the η axis, the order conforms with the order used in the standard finite element region.

The shape functions defined by Eq. (25) can be interpreted in global coordinates by a power series expansion in R_1/R of the form

$$P_i(x, r) = \alpha_1(R_1/R) + \alpha_2(R_2/R)^2 + \cdots + \alpha_q(R_q/R)^q \tag{27}$$

where $\alpha_1, \alpha_2, \ldots, \alpha_q$ are constants and q is determined from the Lagrangian interpolation. Reference to variable order mapped infinite elements relates to the choice of the Lagrangian interpolation and, therefore, to the powers of R_1/R in the asymptotic expansion for the shape function. An expansion of this type with q terms contains a radial basis for spherical Bessel functions up to and including those of order $q - 1$. Therefore, a first-order element ($q = 1$) would be expected to model accurately the radial behavior of an acoustic monopole (standard wave envelope elements correspond to this case), a second-order element to model that of a dipole, and so on. Conceptually this could be extended to any radial order. The higher the order, the more complicated the source representation enabling mapped infinite elements to be introduced closer to the source at the expense of computational time and storage. However, as pointed out in Refs. 3 and 4, there is a limit imposed by the onset of numerical problems related to the ill conditioning of the coefficient matrix if the order is too high ($q > 12$).

Weight Functions

Astley et al.[3] show that, for the boundary integral introduced in the weak formulation to have no contribution on the boundary at infinity, it is necessary for the weighting function of Eq. (1) to be of the form

$$W = Q(\boldsymbol{x})e^{im\theta}[R_1/R(\boldsymbol{x})]^{q+1}\exp\{i\eta_r[\psi(\boldsymbol{x}) - \psi_1]\}$$

$$= D(\boldsymbol{x})P(\boldsymbol{x})e^{im\theta}e^{i\mu(x)} \tag{28}$$

where $q > 1$ and

$$D(\boldsymbol{x}) = [R_1/R(\boldsymbol{x})]^q \tag{29}$$

In the parent element, D can be expressed as

$$D(\xi, \eta) = \left(\tfrac{1}{2}\right)^q(1 - \xi)^q \tag{30}$$

following Eq. (24).

Postprocessing

Variable-order mapped infinite wave envelope elements as already defined provide an approximately reflection free boundary on the interface surface C_r and additionally provide a finite dimensional discretization of the (infinite) far-field region. When implemented as part of an FEM model of acoustic radiation, the discrete equations are in terms of nodal values of the acoustic potential ϕ at the nodes in the standard FEM region and on the interface surface C_r. In the mapped element region, the discrete equations are in terms of nodal values of the function $Q(\boldsymbol{x})$, Eq. (28), which match the nodal values of ϕ on C_r. Postprocessing based on Eq. (15) is required to recover nodal values of acoustic potential in the far-field region. In addition, in the entire computational domain, Eq. (4) is used in postprocessing to obtain the acoustic pressure p.

Kirchhoff Integral Formulation

Once the finite element nodal solution is obtained, the acoustic potential and the acoustic pressure can be postprocessed in the far field (outside C_r) by FEM interpolation using the mapped infinite wave envelope element shape functions. As an alternative, far-field radiation also can be computed using the Kirchhoff method. In the present implementation, the Kirchhoff formula developed by Farassat and Myers[7] for arbitrarily moving and deforming surfaces is used and coupled with the turbofan inlet acoustic radiation code.

For a nondeforming Kirchhoff surface that is in rectilinear motion, the Kirchhoff formula for the acoustic pressure p' at the observer location $\boldsymbol{x}$ and observer time t takes the following form[8]:

$$4\pi p'(\boldsymbol{x}, t) = \int\int_S \left[\frac{E_1}{r_e(1-M_{re})}\right]_{\tau^*} \mathrm{d}S + \int\int_S \left[\frac{p' E_2}{r_e^2(1-M_{re})}\right]_{\tau^*} \mathrm{d}S \tag{31}$$

where

$$r_e = |\boldsymbol{r}_e|, \qquad \boldsymbol{r}_e = \boldsymbol{x} - \boldsymbol{y}(\tau), \qquad \boldsymbol{M}_{re} = \boldsymbol{M}\cdot\boldsymbol{r}_e/r_e \tag{32}$$

$$E_1 = -\boldsymbol{n}\cdot\nabla p' + (\boldsymbol{M}\cdot\boldsymbol{n})(\boldsymbol{M}\cdot\nabla p') + \left[\frac{\cos\gamma - \boldsymbol{M}\cdot\boldsymbol{n}}{c_\infty(1-M_{re})} - \frac{\boldsymbol{M}\cdot\boldsymbol{n}}{c_\infty}\right]\frac{\partial p'}{\partial\tau}$$

$$E_2 = \frac{1-M^2}{(1-M_{re})^2}(\cos\gamma - \boldsymbol{M}\cdot\boldsymbol{n}) \tag{33}$$

where $\boldsymbol{y}$ is the Kirchhoff surface point coordinates, τ is the source time, $\boldsymbol{M}$ is the Mach number vector at which the surface travels, $\boldsymbol{n}$ is the unit normal vector pointing out of the Kirchhoff surface, $\boldsymbol{r}_e$ is the distance from a point on the Kirchhoff surface at the time of emission to the observer at the time of detection, c_∞ is the freestream speed of sound, and γ is the angle between the vectors $\boldsymbol{r}_e$ and $\boldsymbol{n}$ (refer to Fig. 1). The integrands of Eq. (31) are to be evaluated over the Kirchhoff surface at the emission time τ^*, which is given by the root of

$$\tau - t + r(\tau)/c_\infty = 0 \tag{34}$$

For the computational mesh used here, the transitional boundary C_r between the conventional finite elements in the inner region and the mapped infinite wave envelope elements in the outer region, as shown in Fig. 1, serves as the Kirchhoff surface. For proper application of the technique, the Kirchhoff surface should be far enough from the source so that the flowfield is uniform. Because the mapped elements and the transition boundary C_r bordering them lie in a uniform flowfield, this condition is automatically satisfied. The turbofan acoustic radiation code is executed first on a mesh of appropriate resolution composed of conventional finite elements and mapped infinite wave envelope elements of appropriate radial order. In postprocessing of the radiation results, the spatial derivatives of the acoustic pressure in the axial x and radial r directions are computed numerically along the two-dimensional circular transition boundary C_r, which is then rotated about the axis of symmetry to obtain the three-dimensional Kirchhoff surface (sphere). Once the acoustic pressure and its derivatives are defined on the entire Kirchhoff surface, Eq. (31) can be integrated to obtain the pressure at observer locations outside the surface. Further details are available from the study by Spence.[9]

Results and Discussion

Figure 1 shows features of the geometry of a turbofan engine inlet in an x–r plane of a cylindrical coordinate system. The acoustic source on the plane C_f produces a combination of radial modes at a specified angular mode m and nondimensional frequency η_r. The nacelle has a forward velocity specified by the Mach number M_0, which is represented for the stationary nacelle by a steady flow directed toward it. Steady flow into the nacelle is specified by the Mach number M_i, taken to be uniform on the source plane. The steady flowfield inside and outside the nacelle computed on the finite element acoustic mesh provides input data for the FEM acoustic calculations.

Details of the development of mapped infinite elements and demonstration of the considerable improvements achievable in comparison with wave envelope elements in the far field are given in Refs. 5 and 6. Here a typical inlet radiation calculation at relatively high frequency is shown to illustrate how a complex directivity field is resolved using mapped elements in the far field. In addition, it will be shown that the solution can be projected to several far-field regions of varying extent with a single FEM/mapped element

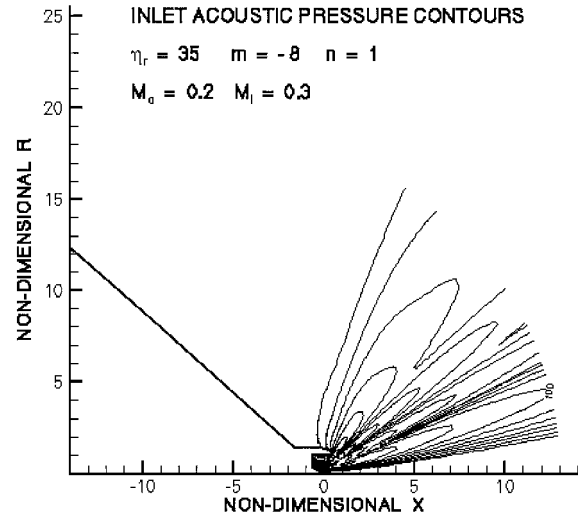

Fig. 4 Isoacoustic pressure contours for generic inlet geometry with acoustic treatment $Z = 2.0 - j\,1.0$, showing substantial scattering from incident $m = -8, n = 1$ mode; far-field region extends to 13 duct radii at the axis of symmetry.

discretization. The example chosen represents a typical blade/vane interaction tone at nondimensional frequency $\eta_r = 35$, angular mode number is $m = -8$, and radial mode is $n = 1$. The inlet Mach number is $M_i = 0.3$ at the source plane and forward flight Mach number is $M_0 = 0.2$. The inlet has acoustic treatment with nondimensional impedance $Z = 2.0 - j\ 1.0$. These conditions produce considerable scattering of the input mode into higher-order radial modes, as can be seen in Fig. 4.

In Fig. 4 contours of sound pressure level over a 55-dB range are shown. The highest level on the outer bounding constant phase circle that intersects the axis of symmetry at a distance of 10 duct radii is arbitrarily set at 100 dB (the 100-dB contour is annotated). Contours are at 5-dB increments. From this example result, it is seen that far-field directivity is very detailed yet well resolved in the FEM/mapped element formulation. Far-field acoustic pressure contours are obtained by postprocessing the acoustic potential solution given at mapped element interpolation nodes via Eq. (15). Contours are generated from an array of evaluation points, which can be extended beyond the region covered by mapped element nodes. Postprocessing need not be limited to the region of FEM/mapped element discretization. Also directly available are directivity on any arbitrary bounding circle and on a sideline, restricted only by the condition that the bounding circle or sideline lie entirely in the far field, mapped element region. Postprocessing to obtain acoustic pressure, in either the near field or far field, requires only spatial derivatives of acoustic potential. Inaccuracies introduced in this operation are minimized either by averaging at element nodes or by postprocessing at Gauss points within elements. No spatial derivatives of acoustic pressure (second spatial derivatives of acoustic potential) are required.

Figure 5 shows sound pressure level for the same FEM/mapped element model shown in Fig. 4, but in this case postprocessed to extend the far-field region to be bounded by a constant phase circle intersecting the axis of symmetry at a distance of 38 duct radii. In this case the far field extends well beyond the region discretized by FEM/mapped element interpolation nodes. Contours are again normalized to 100 dB for the maximum level on the outer boundary, and the 100-dB contour is annotated. Contours are essentially scaled up versions of those shown in Fig. 4, where the outer boundary is at only 13 duct radii (within the region of discretization). Contours of the same decibel level in Figs. 4 and 5 are not exactly the same because normalization is done on different bounding contours. This is particularly noted in the 70-dB contour in Fig. 5 (down 25 dB from the principal lobe), where influence of the baffle begins to appear. The 70-dB contour in Fig. 4 does not show this because with normalization on the 13 duct radii bounding circle the absolute level is higher than the absolute level corresponding to the 70-dB contour of Fig. 5.

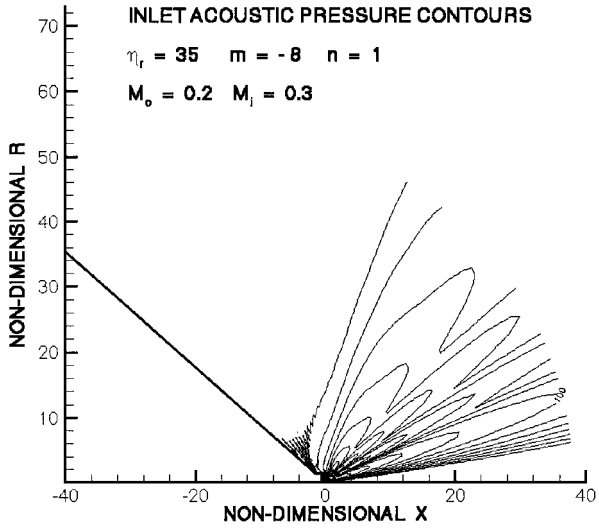

Fig. 5 Isoacoustic pressure contours for generic inlet geometry with acoustic treatment $Z = 2.0 - j\,1.0$, showing substantial scattering from incident $m = -8$, $n = 1$ mode; far-field region extends to 38 duct radii at the axis of symmetry.

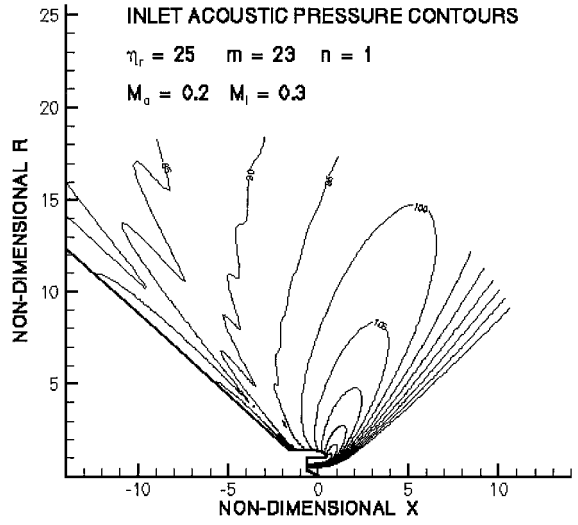

Fig. 6 Isoacoustic pressure contours for generic inlet geometry with incident mode at nondimensional frequency $\eta_r = 25$, incident mode $m = -8$, and $n = 1$; FEM/mapped element computations.

To demonstrate the results obtained by use of the Kirchhoff method and how they compare with those obtained by directly postprocessing the mapped element results in the far field, a second example is considered. Here a case that produces a less complicated far field is considered, to make comparisons more easily interpreted. Inlet radiation is modeled again with standard FEM in the near field and mapped infinite wave envelope elements in the far field. Source and flow conditions are $\eta_r = 25$, $m = 23$, $M_i = 0.3$, and $M_0 = 0.2$ with only the first radial mode incident, $n = 1$. After postprocessing the finite element solution, the acoustic pressure and its derivatives are defined on the transition surface C_r, which serves as the Kirchhoff surface. The Kirchhoff formula is then integrated over the entire Kirchhoff surface to obtain the acoustic pressure at observer points in the far field. It is to be noted here that the transition boundary C_r, when rotated about the x axis to produce the Kirchhoff surface, results in a sphere (with center offset from the coordinate system origin), which does not close in the aft region due to the baffle. The Kirchhoff formula should be integrated over a closed surface to obtain a prediction at an observer point outside the sphere. However, in a previous study, Spence[9] showed that integration over a Kirchhoff sphere open in the aft region is adequate for radiation calculations in the forward radiated far field. Figure 6 shows isoacoustic pressure contours in both near and far field ob-

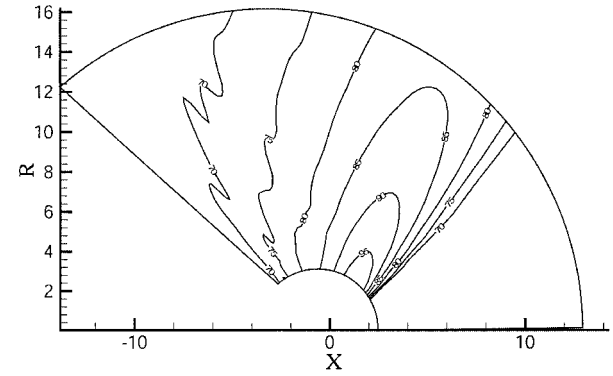

Fig. 7 Isoacoustic pressure contours for generic inlet geometry with incident mode at nondimensional frequency $\eta_r = 25$, incident mode $m = -8$, and $n = 1$; FEM/Kirchhoff calculations.

tained directly from FEM/mapped element postprocessing. Figure 7 illustrates the far-field normalized acoustic pressure magnitude contours resulting from Kirchhoff calculations. No pressure contours inside C_r have been shown because calculation using the Kirchhoff method is justified only outside the Kirchhoff sphere. Furthermore, acoustic pressures inside the Kirchhoff surface are available from the standard FEM operations in this finite region. From a comparison of Figs. 6 and 7, it is apparent that the mapped infinite wave envelope element analysis and the Kirchhoff method predict far-field radiation patterns that are visually similar. Figure 8 plots the magnitude and phase of the complex acoustic pressure from these two analyses on a constant phase circle with an x-axis intercept of 13 duct radii. The magnitude plot indicates that the mapped infinite wave envelope analysis predicts the far-field peak radiation level marginally higher than the Kirchhoff method. Phase angle comparison also is very good except at low and high angles from the axis of symmetry. The acoustic pressures in these regions are relatively low compared to the highest level of radiation.

These results and comparisons demonstrate that mapped infinite wave envelope elements are capable of projecting a near-field acoustic radiation solution to the far field that compares very well with the solution projected using the Kirchhoff integral formula. This postprocessing procedure is a computationally efficient alternative to Kirchhoff calculations. An argument for the use of the Kirchhoff integral method is that it reduces error in the far field, compared with FEM/wave envelope element discretization.[9] However, introduction of mapped infinite elements produces a more accurate far-field approximation than was achievable with standard wave envelope elements. Furthermore, errors introduced must be balanced against errors that occur in calculation of derivatives of the acoustic pressure field on the interface boundary C_r in the Kirchhoff method. These depend on second derivatives of acoustic potential, with the inevitable implications for accuracy. A second unquantifiable source of possible error in the Kirchhoff formulation is the failure to close the Kirchhoff surface at large angles to the axis of symmetry. It is concluded that accuracy in the far field is not necessarily enhanced by use of the Kirchhoff formulation, and in fact, as shown here, the results of the two approaches are in good comparison.

The question of computational efficiency also must be examined. For the example shown in Figs. 7 and 8, the turbofan inlet acoustic radiation code is executed on a computational mesh of 3250 standard finite elements inside C_r and a layer of 75 mapped infinite wave envelope elements outside C_r. For the Kirchhoff method, the mapped infinite wave envelope analysis has to be performed first to define the acoustic pressure and its derivatives on the Kirchhoff surface. Far-field pressure at each observer point is calculated by numerically integrating over 30×150 points on the open Kirchhoff sphere. This results in a total execution time (FEM plus Kirchhoff), which is approximately 2.6 times more than that for the FEM/mapped element analysis alone to produce the result of Fig. 7. Results of Fig. 6 have been generated by carrying the FEM/mapped element procedure to its conclusion with postprocessing to obtain acoustic pressure in the far field based on the mapped elements. Postprocessing time is only a small fraction of the total execution time.

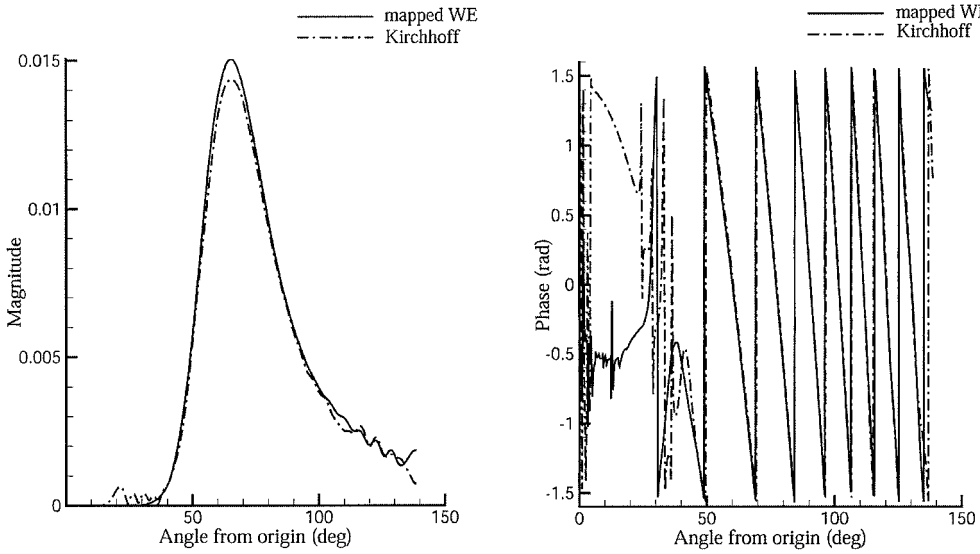

Fig. 8 Acoustic pressure directivity comparison on a constant phase surface at 13 duct radii.

Conclusions

Mapped infinite wave envelope elements provide an effective reflection-free boundary for acoustic radiation from bodies immersed in a uniform steady flow. In addition, these infinite elements provide a finite discretization of the (infinite) far field, which is capable of projecting relatively near-field computations to far-field acoustic pressures with efficient postprocessing. In an application to acoustic radiation from a generic turbofan inlet geometry at relatively high nondimensional frequency and low angular mode number (typical of blade/vane interaction tones), it is found that FEM/mapped elements are capable of producing detailed acoustic pressure radiation patterns representative of substantial scattering in propagation and radiation. Previous studies comparing the performance of wave envelope elements and mapped infinite elements have shown that mapped elements provide a much improved reflection-free boundary for closure of the near-field FEM computational domain. The reflection-free boundary can then be drawn farther into the near field than possible with the older wave envelope elements, and it becomes possible to reduce the dimensionality of the computational domain. It also has been demonstrated that mapped infinite elements provide an efficient means of postprocessing acoustic potential solutions in the near field and projecting acoustic pressure to the far field.

It has been suggested by other investigators that far-field acoustic pressures can be obtained by a postprocessing scheme based on the Kirchhoff integral theorem. The original proposal was that a formulation using FEM and a wave envelope element discretization of the far field be extended to project the near field to the far field. This is attractive because the wave envelope formulation provides no representation of the acoustic field outside the region of FEM/wave envelope discretization. It has been shown here that the FEM/mapped element approach provides the capability to project the solution beyond the region of discretization via simple postprocessing, which is the same used for obtaining the acoustic pressure field in the computational domain.

In the present study, the mapped infinite wave envelope analysis has been supplemented with a Kirchhoff integral method for projecting acoustic radiation patterns in the far field. Comparison of the Kirchhoff method results with that of the mapped infinite wave envelope analysis indicates that the mapped elements are capable of constructing an accurate acoustic wave structure in the far field. The Kirchhoff method produces the complete radiated far field at a much higher computational expense than the mapped element analysis. Therefore, it is concluded that in general it is not necessary to bear the considerable additional postprocessing expense of the Kirchhoff method to obtain useful far-field acoustic radiation solutions.

Acknowledgment

The work reported in this paper was supported by NASA John H. Glenn Research Center at Lewis Field under Grant NAG 3-2109.

References

[1]Parrett, A. V., and Eversman, W., "Wave Envelope and Finite Element Approximations for Turbofan Noise Radiation in Flight," *AIAA Journal*, Vol. 24, No. 5, 1986, pp. 753–760.

[2]Danda Roy, I., and Eversman, W., "Improved Finite Element Modeling of the Turbofan Engine Inlet Radiation Problem," *Journal of Vibration and Acoustics*, Vol. 117, No. 1, 1995, pp. 109–115.

[3]Astley, R. J., Macauley, G. J., Coyette, J.-P., and Cremers, L., "Three Dimensional Wave Envelope Elements of Variable Order for Acoustic Radiation and Scattering. Part I. Formulation in the Frequency Domain," *Journal of the Acoustical Society of America*, Vol. 103, No. 1, 1998, pp. 49–63.

[4]Astley, R. J., Coyette, J.-P., and Cremers, L., "Three Dimensional Wave Envelope Elements of Variable Order for Acoustic Radiation and Scattering. Part II. Formulation in the Time Domain," *Journal of the Acoustical Society of America*, Vol. 103, No. 1, 1998, pp. 64–72.

[5]Eversman, W., "Mapped Infinite Elements for Acoustic Radiation in a Uniformly Moving Medium," *Journal of Sound and Vibration*, Vol. 224, No. 4, 1999, pp. 665–687.

[6]Eversman, W., "A Reflection Free Boundary Condition for Propagation in Uniform Flow Using Mapped Infinite Wave Envelope Elements," *Journal of Computational Acoustics*, Vol. 8, No. 1, 2000, pp. 25–42.

[7]Farassat, F., and Myers, M. K., "Extension of Kirchhoff Formula to Radiation from Moving Surfaces," *Journal of Sound and Vibration*, Vol. 123, No. 3, 1988, pp. 451–460.

[8]Ozyoruk, Y., and Long, L. N., "Computation of Sound Radiating from Engine Inlets," *AIAA Journal*, Vol. 34, No. 5, 1996, pp. 894–901.

[9]Spence, P. L., "Ducted Fan Noise Prediction Using Wave Envelope Analysis and the Kirchhoff Formula," AIAA Paper 97-1651, May 1997.

[10]Eversman, W., and Danda Roy, I., "The Effect of a Baffle on Acoustic Radiation Directivity," AIAA Paper 98-2250, May 1998.

P. J. Morris
Associate Editor